An Experimental Study Of Lorry Rear Side-Skirt And Bumper Flow

Isabel Vallina-Garcia and Holger Babinsky

University of Cambridge

Abstract

A considerable proportion of a lorry's aerodynamic drag is attributed to its underbody. Nevertheless, very few investigations have previously considered the fundamental physics of the underbody flow and hence there is little direction for the effective design of underbody drag-reducing devices. This study investigates experimentally the flow around a lorry rear side-skirt and bumper, using a 1/10th scale lorry model with a detailed, fully reconfigurable underbody and rotating wheels. Testing is conducted in a water tow-tank, which establishes correct ground conditions. The facility operates at a Reynolds Number of approximately Re=6.9x10^5. Optical access into the underbody is possible through the clear working sections of the facility. Stereoscopic Particle Image Velocimetry is used to analyze the flow-field. Force measurements are obtained using a load cell. It is found that flat-plate bumpers increase aerodynamic drag and that a combination of mid and rear side-skirts reduces drag further than mid side-skirts alone. Rear side-skirts have a greater impact when a flat-plate bumper is attached.

1. Introduction

Heavy Goods Vehicles (HGVs) account for approximately 21% of the UK's total fuel consumption [1], despite only representing 5% of the country's total vehicle miles [2]. Due to the associated high fuel costs and the negative environmental impact, commercial operators are trying to reduce their fuel consumption. As shown in Equation 1, for a vehicle travelling at constant speed on flat terrain, fuel consumption is directly proportional to the sum of the aerodynamic drag and the rolling resistance. At European motorway speeds of 90km/h, aerodynamic drag is responsible for approximately 50% of the vehicle's total power requirement [3].

$$F_R = \frac{1}{2}\rho_a V_t^2 C_D A + m_v g C_{rr} \qquad (1)$$

The aerodynamic drag of commercial vehicles is frequently decomposed into four sources: the cab, the cab gap, the rear and the underbody. Although the latter has been attributed 15-30% of the total aerodynamic drag [4, 5], the fundamental physics of the underbody flow have seldom been studied.

Most previous investigations concerning the underbody of HGVs focus on the performance of particular aerodynamic devices. Side-skirts, plastic panels along the sides of the trailer that enclose the underbody, are the most popular. These have been shown to successfully reduce drag [6, 7]. At zero-degree yaw, one drag-reducing mechanism is the prevention of the inward entrainment of high-velocity flow from the vehicle sides into the underbody [8]. Therefore, high-velocity flow continues to move along the trailer sides conserving its energy, instead of generating drag by colliding against bluff underbody components (e.g. the wheel and axle assembly). However, although mid side-skirts (placed between the rear of the tractor and the trailer wheels) have been extensively studied, less consideration has been given to rear side-skirts (placed between the rear of the trailer wheels and the rear of the trailer). These are shown in Figure 1.

Another common underbody component that has not been previously studied in detail is the bumper. Flat-plate bumpers are particularly popular since they effectively reduce spray (see Figure 1). Given that all HGVs are required to be fitted with a bumper and that it has been shown to negatively affect aerodynamic drag [9, 10], it would be useful to improve our understanding of the bumper flow to optimize its design with drag-reduction objectives in mind.

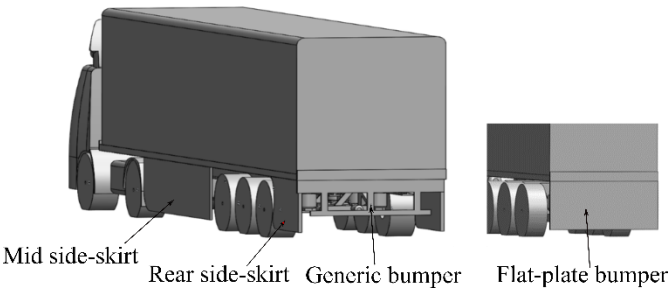

Figure 1. CAD schematic of lorry model with mid and rear side-skirts and generic and flat-plate bumpers.

However, most underbody flow studies so far have tested simple models with clean underbodies in the wind tunnel, where it is difficult to establish correct ground conditions. This work investigates rear side-skirt and bumper flow using a detailed model with an alternative experimental technique in a water tow-tank that correctly establishes ground conditions. This investigation is part of a larger study aiming to gain a better understanding of the underbody flow physics and of flow control strategies to achieve overall drag reductions.

2. Methodology

The experimental work in this study is carried out in the Cambridge University water tow-tank (Figure 2), which is 9m long and has a usable cross section of 1m × 0.8m. The walls and floor of the second working section are made of clear acrylic and those of the third working section of glass, allowing good optical access from all three sides. A 3kW motor, capable of generating 4.7Nm of torque, propels a belt-driven translating carriage to which the model is attached via two vertical rigging bars (in red in Figure 2). These are covered with an aerodynamic fairing to minimize their impact on the flow. A schematic of this fairing is shown in Figure 3. A skim plate spanning the tank width and longer than the model length is attached to the carriage so that its lower face is level with the water's top surface. This maintains a constant water head, considerably reducing the impact on the flow of surface waves.

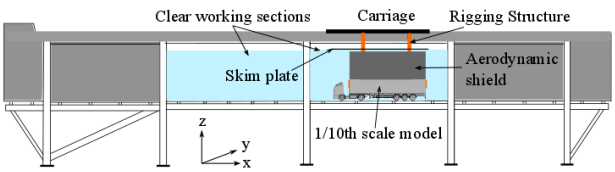

Figure 2. Water tow-tank and model installation. The coordinate system is labelled.

To set up the flow-field, a 1/10th scale lorry model with a detailed underbody and rotating wheels is translated along the tank. A CAD drawing is shown in Figure 4. For each configuration, five runs are performed and ensemble averaged. Measurements are taken at zero yaw-angle. 20 minutes are left between each run to allow turbulent fluctuations to die down. These are reduced to a free-stream level of 0.02%.

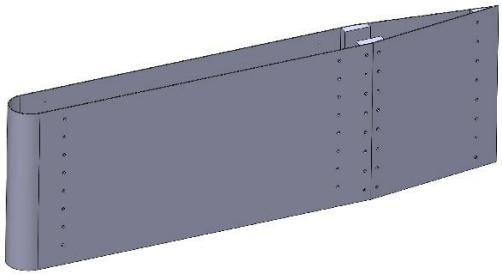

Figure 3. CAD schematic of aerodynamic fairing.

The facility operates at a width-based Reynolds Number in the range of Re_w= $5.97x10^5$ - $7.03x10^5$, depending on the water temperature. Despite being lower than that of a full-scale lorry on the road (approximately $Re_w=4x10^6$) it is of the order of magnitude of the minimum value recommended by SAE guidelines for lorry aerodynamics testing ($Re_w=7 \times 10^5$) [11].

The carriage velocity is controlled through a programmable motor controller. It is measured using a reflective optical sensor that reads a metallic strip with a pattern of rectangular shaped holes spaced out at 1mm. The sensor is connected to an electronic circuit. This generates a high or low voltage output depending on whether the sensor is positioned over a hole or not. This voltage is recorded using a National Instruments USB-6221 Multifunction DAQ data acquisition unit at a rate of 24kHz and is used to calculate the carriage velocity.

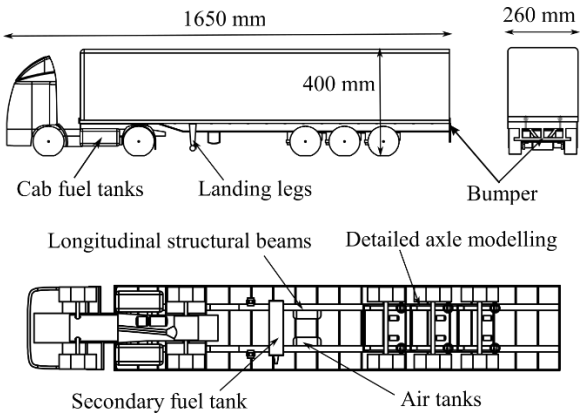

Figure 4. 1/10th scale model (in mm).

The blockage for this experimental setup is 17.5%, a value higher than that usually encountered in aerodynamic investigations. A study on the impact of blockage on the underbody flow of a HGV model in the Cambridge water tow-tank shows that whilst blockage affects local flow velocities and absolute drag forces, global velocity trends are unaffected and flow features are conserved. It is concluded that the flow topology observed is a good representation of on-the-road conditions [12].

This paper presents results from six different underbody setups, illustrated in Figure 5. Configurations I–III test the generic bumper (of the style commonly used by HGVs) with no side-skirts, just mid side-skirts and both mid and rear side-skirts respectively. Configurations IV–VI test the flat-plate bumper with no side-skirts, just mid side-skirts and both mid and rear side-skirts respectively. Configuration I is referred to as the baseline. For configurations II–VI, the normalized height of the flat-plate bumper (h_{bpr}/h) and the mid and rear side-skirts (h_{ss}/h) varies in the range 26.1–76.5% (see Figure 6).

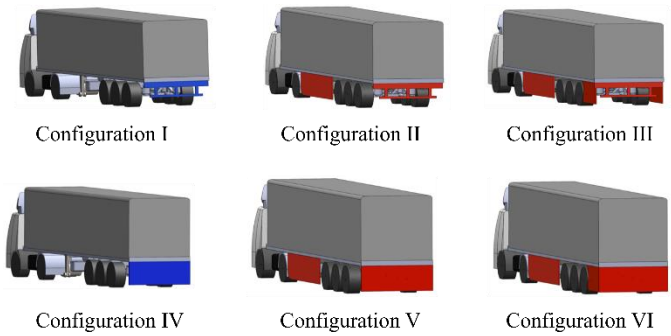

Figure 5. Underbody configurations studied.

A load cell and stereoscopic Particle Image Velocimetry (SPIV) are used to study the flow-field. The SPIV setup allows three-component velocity vectors to be measured in 3D space.

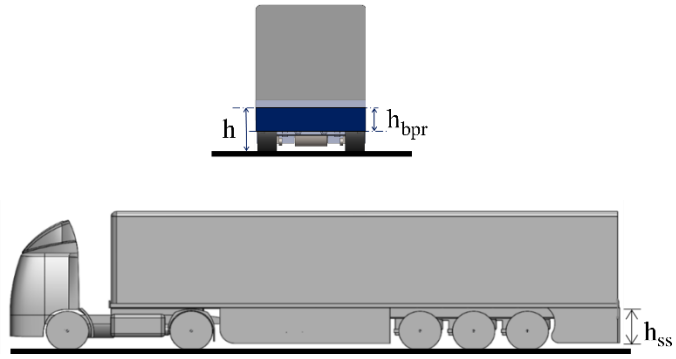

Figure 6. Flat-plate bumper and mid and rear side-skirts tested for range of normalized heights.

2.1 Load Cell

Load measurements are taken with a specially designed balance [12] bolted to the towing carriage as in Figure 7. It allows accurate force measurements in the drag direction while withstanding the large pitching moments and buoyancy force experienced by the rigging apparatus.

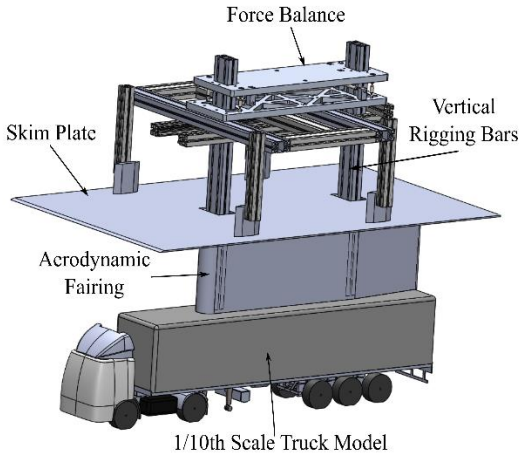

Figure 7. Balance rig.

The balance is calibrated attaching a wire to the rear rigging bar from which known loads are hung via a pulley (Figure 8). The average voltage measured for each load, during loading and unloading, is recorded. The on-axis hysteresis is 0.3% of the total load.

Before each test, a zero reading is taken and subtracted from the measured loads to remove drifts caused by environmental changes, like temperature effects. To calculate the drag coefficient (C_D) for each configuration, the sample points within the measurement region are divided by their instantaneous velocity squared and time-averaged over the measurement region. The datasets for the different runs are ensemble-averaged. ΔC_Ds between each setup and the baseline are calculated. A positive ΔC_D indicates a drag increase.

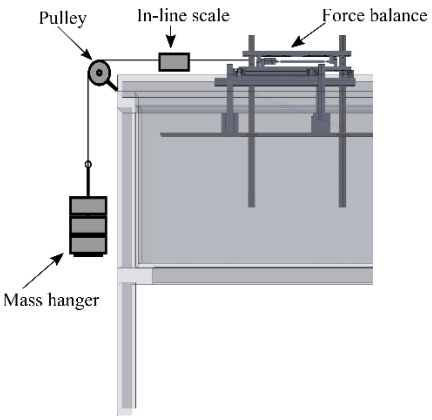

Figure 8. Load cell calibration setup.

2.2 High-Speed PIV System

Particle Image Velocimetry (PIV) is an unobtrusive, optical technique that relies on tracer particles. Via the statistical analysis of the particle field, the flow velocity field is determined. The particles are illuminated in a particular plane and photographed at high speed. Cross-correlation techniques are used to process the resultant sequential images to obtain velocity vectors.

A PIV system supplied by LaVision is used, comprising a double-cavity high-speed laser with an output of 30mJ per pulse per cavity at 1kHz at a wavelength of 527nm. Its maximum frequency is 20kHz. Two Phantom Miro 310 high-speed cameras with a maximum resolution of 1280x800px are used to obtain stereoscopic data. Titanium dioxide particles with a characteristic diameter of 45µm seed the flow. Images are checked for peak locking, ensuring that particles are smeared over several pixels. It is verified that the probability density function of the processed velocity field shows no tendency towards integer velocities.

For the stereoscopic PIV setup (see Figure 9), an optical guiding arm guides the laser beam underneath the water tank. It is intercepted by sheet forming optics that generate a vertical light sheet perpendicular to the model's direction of motion. The light sheet is 4-5mm thick and is aligned to the measurement plane with an accuracy of ±1mm. The two high-speed cameras are focused on the light sheet, one upstream and one downstream, at an angle of approximately 37.5º.

The cameras are fitted with Scheimpflug adaptors to adjust the focal plane angle so that it remains parallel to the measurement plane. To prevent refraction effects, the cameras look through a water-filled prism attached to the tow-tank underside. The acquisition frequency is 3kHz so a seeding particle remains in the laser sheet for several frames before moving out in the streamwise direction. A PIV processing window of 32x32px with 50% overlap is used. Two passes are performed on the data. Each SPIV result is formed of an ensemble average of five experimental runs. Results are also averaged in blocks of 5 in the streamwise direction. This reduces the streamwise resolution from 1mm to 5mm but increases the number of averages. Underbody components sometimes obstruct a camera's

view of the seeding particles, leading to the generation of incorrect vectors. These are filtered out using a mask that simulates the cameras' vision [12]. PIV data is plotted using velocity contours on vertical plane x/b=6.35 (see Figure 10).

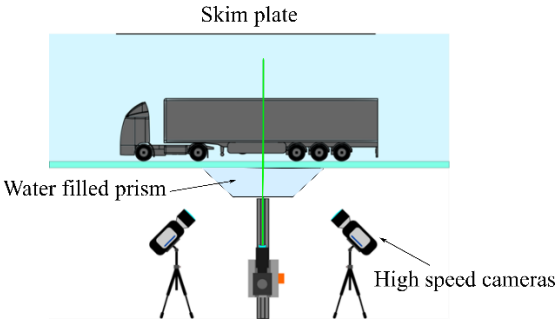

Figure 9. Stereoscopic PIV setup.

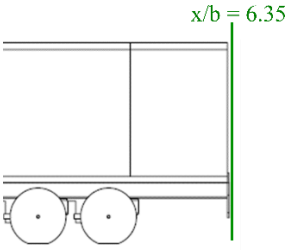

Figure 10. SPIV measurement plane: x/b=6.35.

3. Results & Discussion

3.1 Bumper Flow

Configuration IV, where the normalized height of the flat-plate bumper is varied between 26.1–76.5%, is tested. Figure 11 plots ΔC_D relative to the baseline case against normalised bumper height. The baseline is shown in red.

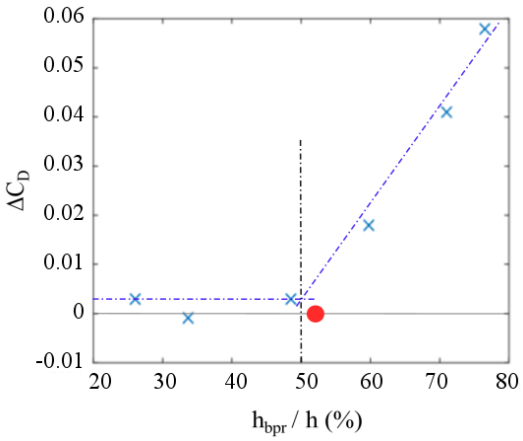

Figure 11. ΔC_D vs h_{bpr}/h for Configuration IV relative to I. Baseline in red.

Overall, ΔC_{DS} are positive. Therefore, flat-plate bumpers increase drag relative to the generic design. Drag decreases linearly with bumper height until $h_{bpr}/h \approx 50\%$. For ground clearances greater than this, the drag remains relatively constant and approximately equal to the baseline's. Therefore, there appears to be a 'critical height' for flat-plate bumpers, below which there is no additional drag penalty.

This trend may be explained considering the bumper location at the vehicle rear. Figure 12 shows normalised streamwise velocity contours on plane x/b=6.35 for a configuration with no bumper. Closer to the ground, the flow velocity is higher and approximately equal to half of the free-stream's. A bumper protruding in this region would considerably decelerate the flow and so, increase drag. However, for z/b>0.3, the flow velocity is much lower. A bumper in this region does not impact vehicle drag significantly.

It is likely that the critical bumper height depends on the underbody geometry. Particularly, on the height of the lowest protruding underbody component. For the model tested, most components have a normalised height shorter than 0.45.

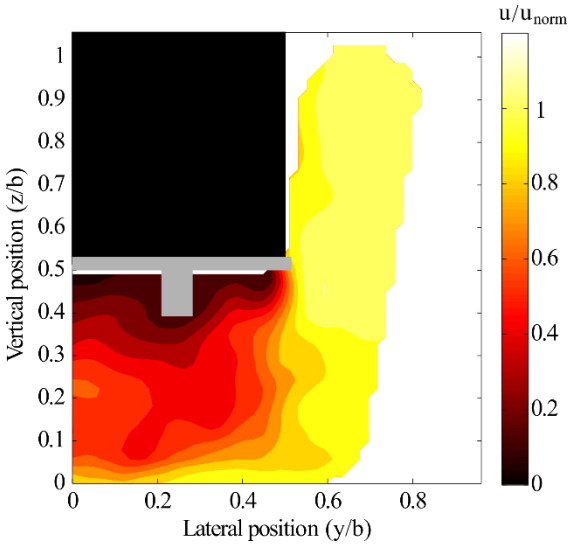

Figure 12. Normalised streamwise velocity contours on plane x/b=6.35 for configuration with no bumper.

3.2 Rear Side-Skirt Flow

Configurations II and III are tested, where the normalised height of mid side-skirts or of both mid and rear side-skirts respectively is varied in the range 26.1–76.5%. To isolate the impact of rear side-skirts on vehicle drag, the ΔC_D between Configurations II and III at each skirt height is found. Figure 13 plots ΔC_D for Configuration III relative to II against normalised skirt height.

For all h_{ss}/h, ΔC_{DS} are negative, indicating that rear side-skirts decrease drag further. Shorter rear side-skirts are slightly more effective. However, the drag reductions are very small, the changes being equal to or smaller than the measurement technique's experimental error (±0.01). Therefore, rear side-skirts do not significantly impact drag when the generic bumper is attached.

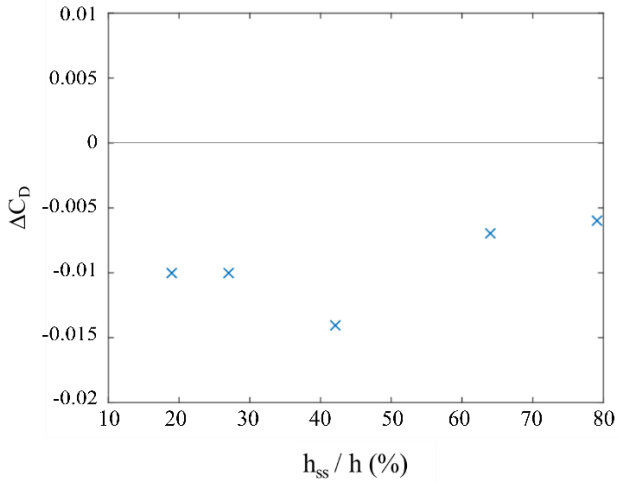

Figure 13. ΔC_D vs h_{ss}/h for Configuration III relative to II.

Rear side-skirts may decrease drag in a similar way to mid side-skirts, reducing inward flow entrainment onto the bumper. However, we found that short bumpers do not significantly increase drag, since the surrounding flow already has relatively low velocity. Therefore, an alternative drag-reduction mechanism seems likely. One hypothesis is that rear side-skirts affect base pressure. McAuliffe [13] showed that rear side-skirts raise the pressure across the trailer base. This may not be measured directly with the current experimental setup.

3.3 Rear Side-Skirt & Bumper Interaction

To improve our understanding of the rear side-skirt and bumper flow, tests analogous to those in section 3.2 are conducted for Configurations V and VI, where a flat-plate bumper replaces the generic design. Figure 14 plots ΔC_D for Configurations II-VI relative to the baseline case, when $h_{bpr}/h=h_{ss}/h=76.5\%$.

As expected, mid side-skirts in Configuration II decrease drag relative to the baseline (ΔC_D = -0.0285). Rear side-skirts in Configuration III reduce drag further, although significantly less (an additional ΔC_D = -0.0060). When the generic bumper is replaced by the flat-plate bumper in Configuration IV, drag increases considerably. This agrees with the bumper being taller than the critical height of $h_{bpr}/h\approx50\%$.

When mid side-skirts are attached to Configuration V, a drag reduction is observed relative to Configuration IV (ΔC_D = -0.0280). It is interesting that mid side-skirts achieve similar drag reductions irrespective of the bumper design. This suggests that mid side-skirts have no additional impact on the flow at the vehicle rear.

When rear side-skirts are attached to setup VI, a ΔC_D=-0.0280 is measured relative to Configuration V. Therefore, the drag reduction attributed to rear side-skirts is more than four times greater with the flat-plate bumper than the generic. As discussed in section 3.2, it is possible that rear side-skirts raise base pressure. Given that flat-plate bumpers increase the base area, the rise in pressure is applied to a greater surface area. Therefore, a greater reduction is expected.

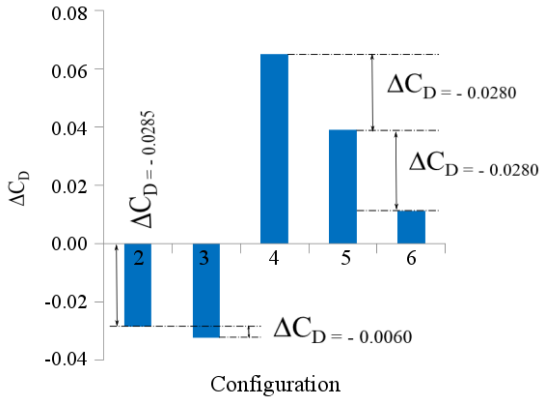

Figure 14. ΔC_D for configurations II–VI relative to the baseline for $h_{bpr}/h = h_{ss}/h = 76.5\%$.

4. Conclusions

This study uses a water tow-tank and a detailed 1/10th scale lorry model to investigate rear side-skirt and bumper flow. Load cell measurements indicate that flat-plate bumpers taller than $h_{bpr}/h\approx50\%$ increase aerodynamic drag considerably. For bumpers shorter than this critical height, no additional drag penalty is measured. This critical height is thought to depend on the specific underbody configuration, particularly on the height of the lowest protruding underbody component. This suggests that flat-plate bumpers shorter than $h_{bpr}/h\approx50\%$ may be used to reduce spray with minimal impact on drag.

Rear side-skirts reduce drag further, although to a lesser extent than mid side-skirts. Rear side-skirt performance seems dependent on bumper geometry, being most efficient with the flat-plate bumper.

References

1. Gregory, M., Khan, S., “Sub-National Road Transport Fuel Consumption Statistics,” Department of Energy and Climate Change, 2014.
2. Heyworth, A., “Annual Road Traffic Estimates: UK 2012,” Department for Transport, 2013.
3. Hakansson, C., Lenngren, M.J., “CFD Analysis of Aerodynamic Trailer Devices for Drag Reduction of Heavy Duty Trucks,” Chalmers University, 2010.
4. Cooper, K., "The Wind Tunnel Testing of Heavy Trucks to Reduce Fuel Consumption," SAE Technical Paper, 1982.
5. Drollinger, R., "Heavy Duty Truck Aerodynamics," SAE Technical Paper, 1987.
6. Cooper, K., “Wind Tunnel and Track Tests of Class 8 Tractors Pulling Single and Tandem Trailers Fitted with Side-Skirts and Boat-tails,” SAE International Journals, 2012.
7. Ortega, J.M., Salari, K., “An Experimental Study of Drag Reduction Devices for a Trailer Underbody and Base,” AIAA Conference, 2004.
8. Stephens, R., Babinsky, H., “An Experimental Study on Truck Side-Skirt Flow,” SAE International Journals, 2016.

9. Van Raemdonck, G.M.R., Van Tooren, M.J.L., “Design of an Aerodynamic Aid for the Underbody of a Trailer Within a Tractor-Trailer Combination,” BBAA International Colloquium on Bluff Body Aerodynamics, 2008.
10. Storms, A., “A Summary of the Experimental Results for a Generic Tractor-Trailer,” NASA, 2006.
11. Truck and Bus Aerodynamics and Fuel Economy Committee, “Wind Tunnel Test Procedure for Trucks and Buses,” SAE Standard J1252_201207, 2012.
12. Stephens, R.G., “Water Towing Tank Investigation of the Underbody Aerodynamics of a Heavy Goods Vehicle,” Cambridge University, 2017.
13. McAuliffe, B.R., D’Auteuil, A., “A System for Simulating Road-Representative Atmospheric Turbulence for Ground Vehicles in a Large Wind Tunnel,” SAE International Journals, 2016.

Nomenclature

ρ_a	Water density
A	Model frontal area
b	Model width
C_D	Drag coefficient
C_{rr}	Rolling coefficient
F_R	Total road force
g	Gravitational acceleration
HGV	Heavy Goods Vehicle
h_u	Underbody height
m_v	Vehicle mass
Re_w	Width-based Reynolds number
SPIV	Stereoscopic Particle Image Velocimetry
V_t	Vehicle speed